NMR, x-ray, and Mössbauer results for amorphous Li-Si alloys using density functional tight-binding method

F. Fernandez [1,2] M. Otero [1,2] M. B. Oviedo [3,4] D. E. Barraco [1,2] S. A. Paz [3,4,*] and E. P. M. Leiva [3,4]

[1] *Facultad de Matemática, Astronomía, Física y Computación, Universidad Nacional de Córdoba, Córdoba X5000HUA, Argentina*

[2] *Consejo Nacional de Investigaciones Científicas y Técnicas (CONICET), Instituto de Física Enrique Gaviola, Córdoba X5000HUA, Argentina*

[3] *Facultad de Ciencias Químicas, Departamento de Química Teórica y Computacional, Universidad Nacional de Córdoba, Córdoba X5000HUA, Argentina*

[4] *Consejo Nacional de Investigaciones Científicas y Técnicas (CONICET), Instituto de Fisicoquímica de Córdoba (INFIQC), Córdoba X5000HUA, Argentina*

(Received 22 May 2023; revised 23 August 2023; accepted 12 September 2023; published 2 October 2023)

Silicon anodes hold great promise for next-generation Li-ion batteries. The main obstacle to exploiting their high performance is the challenge of linking experimental observations to atomic structures due to the amorphous nature of Li-Si alloys. We unveil the atomistic-scale structures of amorphous Li-Si using our recently developed density functional tight-binding model. Our claim is supported by the successful reproduction of experimental x-ray pair distribution functions, NMR, and Mössbauer spectra using simple nearest-neighbor models. The predicted structures are publicly available.

DOI: 10.1103/PhysRevB.108.144201

I. INTRODUCTION

Global warming caused by fossil fuel burning appears as the biggest environmental problem facing us in this century. One of its major contributions is due to the use of internal combustion vehicles, so a transition to electric vehicles maintaining autonomy and charging time are of vital importance along with habit changes. One of the goals set by the Intergovernmental Panel on Climate Change (IPCC) is to limit the average temperature increase to 1.5 °C. This requires changes in technology and human behavior, one of the most important of which is that by 2050, 80% of energy must be supplied by renewable sources [1]. Next-generation lithium batteries are the most promising option to meet the intermittency of renewable energies and power electric vehicles, but they require an increase in their capacity. In this sense, silicon anodes are presented as the best candidate because of the high theoretical capacity of 3579 $mAhg^{-1}$, which is ten times higher than the current graphite anodes, besides being a cheap, abundant, and environmentally friendly material. However, it presents large volumetric changes, of the order of 300%, which lead to structural degradation and a consecutive capacity lost in successive charge/discharge cycles [2].

It has been shown [3] that knowledge at the atomic level of the batteries' active materials allow designing strategies that mitigate their limitations and greatly improve performance. This has inspired the scientific community to apply numerous microscopic and spectroscopic characterization techniques. The intrinsic behavior of Si anodes leads to the formation of amorphous Li-Si alloys during charge/discharge that make the short-range structure especially relevant. It has been stated that the crystal-amorphous phase transition occurring for this system represents the main obstacle to improving its electrochemical performance, mainly because it hinders the attempts to link the atomic structures with the experimental observations [4]. Although there are experiments related to local structures such as nuclear magnetic resonance (NMR), Mössbauer spectroscopy (MB), x-ray pair distribution function (PDF), among others, their interpretation is evasive without a precise theoretical model capable of predicting the microscopic structure of the system and correlate it with the experimental observables. As an example, two different states of Li ions are always observed, and an intermediate transition that has not yet been elucidated, in voltammograms [5], in diffusion coefficients [6], and in NMR experiments [7].

In previous work, we parametrized a density functional tight-binding (DFTB) potential that exhibits a remarkable precision in the prediction of the formation energies for several Li_xSi crystalline and amorphous structures, in a wide range of compositions [8]. Furthermore, using this potential, the simple annealing of crystalline silicon (*c*-Si) resulted in an amorphous structure (*a*-Si) with a radial distribution function (RDF) that is in perfect agreement with experimental results [9]. In light of these results, we show here that the amorphous structures predicted by our model can be used to understand NMR [4,7,10,11], MB [12], and x-ray PDF [13] experimental measurements using a simple nearest-neighbor model.

II. COMPUTATIONAL METHODS

We started by lithiating the *a*-Si structure obtained in our previous work [8], following a procedure similar to that proposed by Chevrier and Dahn [14]: (i) Add a Li atom at the

*apaz@unc.edu.ar

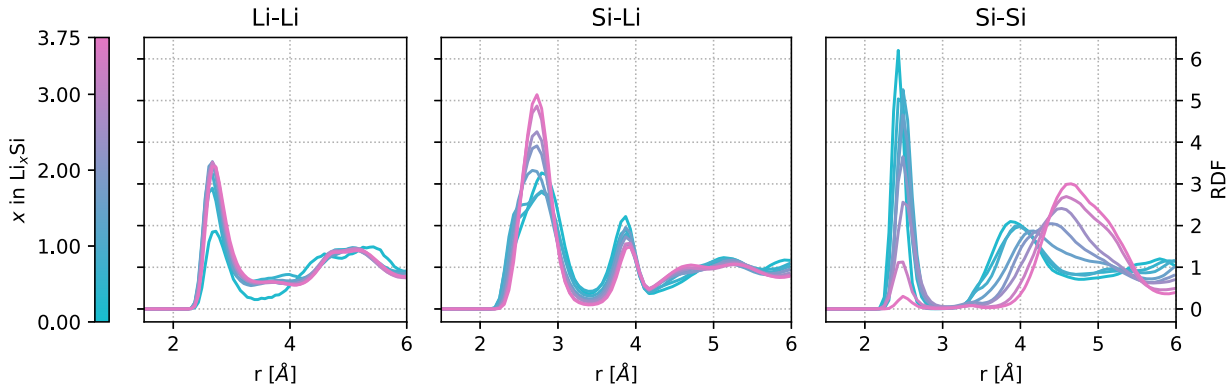

FIG. 1. Partial RDF for Li-Li, Si-Li, and Si-Si for the optimized x values of 0.20, 0.56, 0.89, 1.50, 2.00, 2.50, 3.28, 3.75 in Li_xSi. The color of the curve changes from cyan (Si predominance) to pink (Li predominance). In Fig. S1 of the Supplemental Material [17] we present this information without curves overlapping. Error bars are smaller than the linewidths.

center of the largest spherical void, increase the volume, and scale coordinates by a factor to obtain the experimental expansion in the system. (ii) Perform an *NPT* molecular dynamics equilibration for 10 ps using the Berendsen thermostat and barostat [15] available in the DFTB+ code [16]; repeat these two steps until the desired number of Li atoms is reached. Step (ii) represents a slight modification that improves the fixed-volume coordinate optimization procedure performed at Ref. [14]. Following this procedure, we obtain amorphous structures for a wide range of Li_xSi concentrations, from the initial 64 Si atoms ($x = 0$) to a total of 304 for the fully lithiated structure ($x = 3.75$). Note that other computational methods to obtain amorphous structures are possible, such as simulated annealing as discussed in the Supplemental Material [17] (see Fig. S3 and Refs. [8,18] therein). All the observables at each particular x value computed in this work were calculated using a longer trajectory of 0.5 ns. The optimized x values are 0.20, 0.56, 0.89, 1.50, 2.00, 2.50, 3.28, 3.75. These structures are available in a public repository [19].

III. RESULTS

A. X-ray pair distribution function

First, we characterize the amorphous structures by computing the partial radial distribution functions (RDFs), which describe the probability of finding an atom in a shell at a distance r from a reference atom and are described in Eqs. (S1)–(S3) of the Supplemental Material [17]. As can be seen in Fig. 1, the nature of the obtained distributions is typical for amorphous structures, having a well-defined first peak at short r and decreasing the following ones for increasing r. The most interesting behavior to analyze is found in the Si-Si RDF. As the lithium concentration increases there is clearly a decrease in the first neighbor peak together with a shift in the second neighbor peak towards larger distances (3.8 Å → 4.7 Å). This tells us that the Si-Si bonds are being broken during the lithiation and isolated Si appears. It is worth mentioning that the DFTB model used in this work allows us to capture these fine chemical features at a low computational cost, showing great detail in the representation of the electronic structure of many atoms (see Supplemental Material [17] and corresponding Refs. [20–25]).

Combining the previous partial RDFs allowed us to calculate the total $G(r)$ for each structure, as detailed in the Supplemental Material [17]. The $G(r)$ can be directly compared with the PDF obtained from x-ray measurements [26]. The triangles of Fig. 2 show the x-ray PDFs for the two extreme cases of unlithiated a-Si (bottom) and full lithiated silicon anode (top), as measured by Laaziri *et al.* [9] and Key *et al.* [4], respectively. For comparison, we include in the same figure the $G(r)$ computed using the following procedures. For a-Si, we directly take the $G(r)$ as an average from our a-Si modeled structures, resulting in an excellent agreement with the experimental measurement, as can be seen at the bottom of the figure. For the case of the fully lithiated silicon anode, the experimental sample is expected to be mainly composed of amorphous $Li_{15}Si_4$, although a crystalline contribution to the x-ray PDF may also be expected. In addition, another

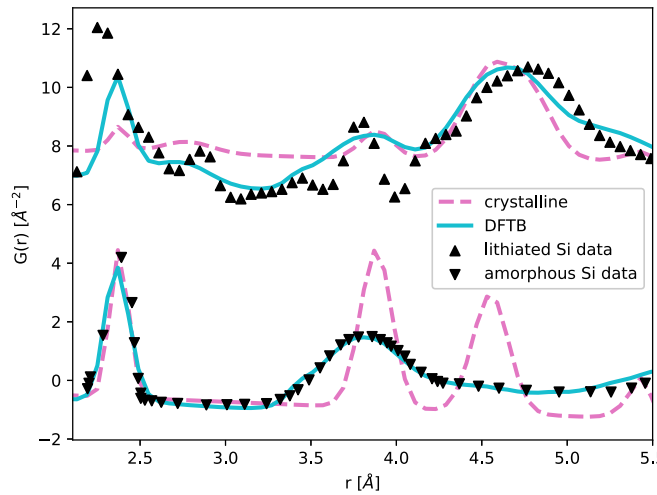

FIG. 2. Pair distribution functions $G(r)$ for amorphous and full lithiathed Si contrasted with experimental data. The triangles pointing down correspond to Laaziri's a-Si experiment [9], while those pointing up correspond to Key *et al.*'s experiment [4]. The DFTB cyan curves consider both crystalline and amorphous structures. The contributions of each one are given in Table S1 of Supplemental Material [17]. The lithiated Si data have an extra contribution of 8 Å^{-2} to have the two curves in the same plot. Error bars are smaller than the linewidths.

contribution from pure Si is also possible, mainly due to an incomplete lithiation resulting from various experimental factors such as bad connectivity, kinetically limited events, or even a possible $Li_{15}Si_4$ decomposition [4,7]. Therefore, we have fitted the experimental data shown in Fig. 2 using a linear combination of the $G(r)$ obtained from the a-$Li_{15}Si_4$ and a-Si modeled structures, but also including the crystalline ones (see Supplemental Material [17]). Strikingly, the resulting weights for the crystal phases are quite small, representing only a 9.78% for c-$Li_{15}Si_4$ and exactly 0% for c-Si. This highlights the importance of taking into account amorphous atomic structures to understand the experimental measurements. On the contrary, a very poor fit is obtained if only crystal structures are used, as can be seen at the top of Fig. 2 (pink curve). Note that there is a significant improvement with respect to previous fit by Key *et al.* [7]. However, there are some features in the experimental measurement, such as the peak at 3.5 Å, that are not completely described and require further analysis.

B. ^{7}Li NMR chemical shift

A direct measurement of the local atomic structure is challenging, however, some spectroscopic techniques allow us to infer the local structure due to a high dependence of the measured property on the atomic local environment. This is the case for NMR and MB spectroscopy. In previous work, Key *et al.* [7] prepared different Li-Si structures and measured their ^{7}Li NMR chemical shift spectra. A NMR spectrum is the sum of the signal contributions coming from all ^{7}Li in the structure, with chemical shifts that depend on their local environments. In this spectra, Key *et al.* [7] assigned a peak at 18 ppm to the chemical shift of a ^{7}Li atom which is near a bonded Si atom. On the other hand, a peak at 6 ppm was attributed to ^{7}Li near an isolated Si atom. However, it is not clear how to interpret the occurrence of peaks between 6 and 18 ppm, which are in fact observed in the NMR measurements. We propose here a simple nearest-neighbor model to emulate and interpret these features in the NMR spectra.

First, we define the chemical shift of the ith Li atom as

$$\delta_i = \frac{1}{N_i^{\mathrm{Si}}} \sum_{\alpha}^{N_i^{\mathrm{Si}}} \delta_{\mathrm{Key}}(\alpha), \tag{1}$$

where

$$\delta_{\mathrm{Key}}(\alpha) = \begin{cases} 18 \text{ ppm} & \text{if } \alpha \text{ is a bonded Si atom,} \\ 6 \text{ ppm} & \text{if } \alpha \text{ is an isolated Si atom,} \end{cases} \tag{2}$$

Equation (2) is the mathematical formulation of the hypothesis put forward by experimentalists [7] which assumes that the chemical shifts are produced by essentially two categories of Li ions: those that are close to Si atoms that are bonded to other Si atoms (18 ppm), and those that are close to isolated Si atoms (6 ppm).

The sum in (1) considered over the Si nearest neighbors of the ith atom (N_i^{Si}) and δ_{Key} is defined considering the shifts proposed by Key *et al.* [7], as discussed above. The nearest neighbors are determined by considering a cutoff distance that is chosen as the position of the minimum between the first and second peak in the corresponding partial RDF. The cutoff is 3 Å for Si-Si and 3.4 Å for Li-Si.

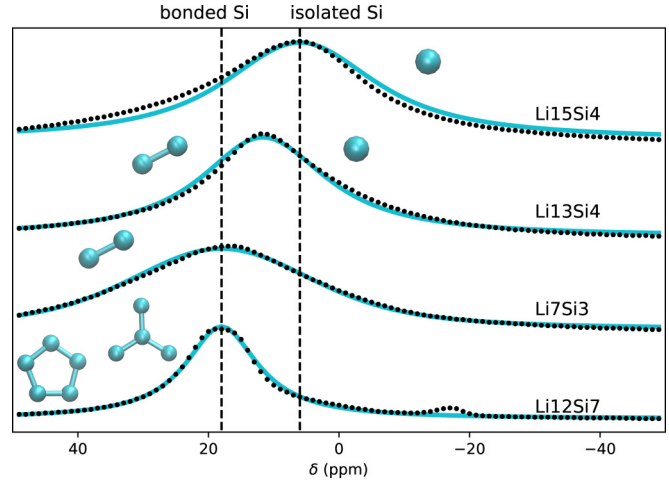

FIG. 3. ^{7}Li chemical shift spectra for crystalline alloys. The dots correspond to the measurements of Key *et al.* [7] and the solid lines to the present nearest-neighbor model. Vertical lines indicate the contributions of bonded and isolated Si. Error bars are smaller than the line widths.

The total NMR spectrum is built as a histogram of peaks whose positions are given by Eq. (1). We generate this histogram using a sum of Voigt kernels V centered at δ_i over all the Li atoms in the structure,

$$I(x) = \sum_i V(x, \delta_i, \sigma, \gamma), \tag{3}$$

where x is the chemical shift, σ is the standard deviations of the Gaussian component due to the detector, and γ is the half width at half maximum of the Lorentzian component that is intrinsic to the NMR phenomena. Finally, an average was taken over all snapshots of our molecular dynamics trajectories. Parameters of the fitted Voigt kernels are provided in Table S2 of the Supplemental Material [17].

As a first test of this model, we present the ^{7}Li chemical shift spectra for the crystalline structures in Fig. 3, as calculated from the present assumptions. The atomic configurations were obtained from the Materials Project [27] and the peak width was fitted to the accuracy of the Key *et al.* experiment [7] once the nearest-neighbor model determined the center of the peak. The model presented here corresponds to the continuous lines, while Key's measurements correspond to the points. For all four alloys, the center of the peak is reproduced with high accuracy. In the $Li_{12}Si_7$ and Li_7Si_3 alloys, the Si atoms are all bonded. The first forms pentagons of five atoms or stars of four, while in the second one, all the bonds are dumbbells. This shows that in this nearest-neighbor model, all the Li atom contributions are centered at 18 ppm. In the fully lithiated alloy $Li_{15}Si_4$ there are only isolated Si atoms, so all the contributions are centered at 6 ppm. Meanwhile, for $Li_{13}Si_4$, isolated Si coexists with dumbbells, making intermediate contributions to the spectra, consistent with experiment.

Having obtained these promising results for the crystalline structures, we now focus on amorphous structures, which are usually found in electrochemical experiments. We calculate the ^{7}Li chemical shift spectra for different amorphous Li-Si alloys with the proposed nearest-neighbor model using the

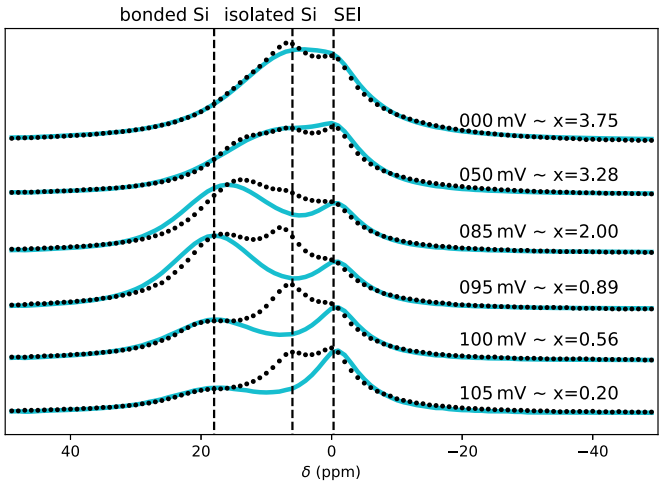

FIG. 4. ^{7}Li chemical shift spectra for amorphous structures. The dots correspond to the measurements of Key *et al.* [7]. The results of the present model are represented with solid lines and a SEI contribution is added for comparison. The vertical lines indicate the contributions of SEI and bonded or isolated Si atoms. Error bars are smaller than the linewidths. Discrepancies at 6 ppm may be due to nonhomogeneous lithiation in experiments as explained in Ref. [7].

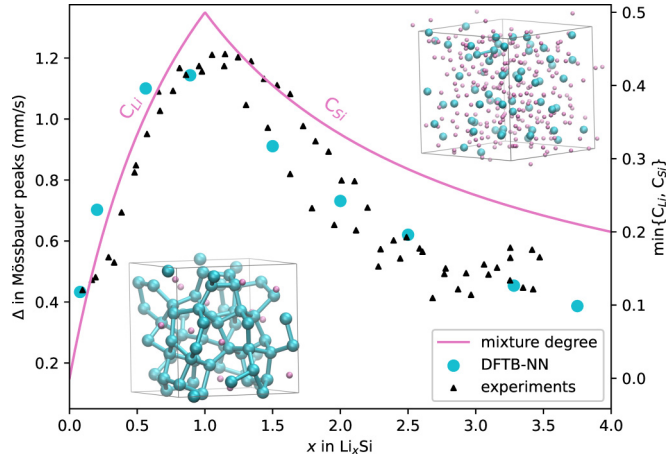

FIG. 5. Shift between the two peaks in the Mössbauer effect spectra. The triangles pointing up correspond to two measurements from Li *et al.* [12] (left axis), the solid line is the prediction of Eq. (5), using average concentrations of Li and Si atoms. The cyan circles are the prediction given by Eq. (5), with C_{Li}, C_{Si} calculated from the nearest-neighbor concentration (right axis). Error bars are smaller than the size of the points.

structures obtained from our molecular dynamics simulation. We considered those structures with x values in $\mathrm{Li}_x\mathrm{Si}$ that can be related to the voltages used by Key *et al.* [7] to collect the NMR spectra. To facilitate the comparison with our model we have included a peak at -0.3 ppm, which represents the solid electrolyte interphase (SEI) contribution, as suggested by the cited authors. The results are shown in Fig. 4 which, apart from some differences explained below, show a reasonable agreement between the computational and experimental results. This is particularly true in the case of the peak at 18 ppm, where the modeling is able to mimic the shift of the peak to 6 ppm at high concentration. This change is the clearest evidence to support the current atomistic view of the system. At the beginning of the lithiation, the configurations contain mainly bonded Si atoms. Then there is an intermediate coexistence between bonded and isolated Si atoms. Finally, isolated Si atoms prevail at high lithium concentrations.

There is a better agreement between the model and experiment at high Li concentrations. At low Li concentrations, our model results show a major discrepancy with the experimental results. However, this should not be attributed to a model limitation but rather to the experimental lithiation being highly inhomogeneous [7]. That is, the extra contribution to the experimental spectrum at 6 ppm is attributed to isolated Si atoms in highly lithiated regions which we do not include in our model. Our simulations correspond to structures in thermodynamic equilibrium and do not take into account these highly lithiated metastable phases that appear in the Key *et al.* experiments for low overall lithium concentrations [7].

C. Mössbauer spectroscopy peak splitting

A different perspective on the study of local atomic structure was provided by Li *et al.* [12]. They used gamma rays to measure the ^{119}Sn Mössbauer spectra (MB) of amorphous $\mathrm{Li}_x\mathrm{Si}_{1-y}\mathrm{Sn}_y$, for $0 < x < 3.5$ and small values of y [12]. Given the low concentration of tin, the authors assume that Sn atoms occupy the same sites of Si atoms in this material, making it equivalent to the result of an amorphous Si lithiation [28]. The MB signal consists of two peaks that almost completely overlap at the extreme cases of low or high lithium concentration, but are clearly separated for the intermediate cases. The separation distance Δ is expected to be sensitive to the local environment of Sn atoms. Δ reaches a maximum value around 1.2 mm/s at $x \sim 1$ and decreases for lower and higher concentrations (see triangles in Fig. 5). The authors suggest that the maximum value of Δ is obtained when Sn atoms (and by analogy Si atoms) are surrounded by an equimolar mixture of Si and Li, and then decreases when some of the two atom types predominate. In order to make a quantitative statement in terms of this idea, let us define the concentration of Li atoms, say C_{Li}, and the concentration of Si atoms, say C_{Si}, in terms of the number of Li atoms in the formula $\mathrm{Li}_x\mathrm{Si}$:

$$C_{\mathrm{Li}} = \frac{x}{1+x}, \quad C_{\mathrm{Si}} = 1 - C_{\mathrm{Li}}. \tag{4}$$

Now, since we find from the experimental results in Fig. 5 that Δ tends to a constant value at small and large x values, we propose for Δ the following ansatz:

$$\Delta = a \min\{C_{\mathrm{Li}}, C_{\mathrm{Si}}\} + b. \tag{5}$$

By tuning the a and b coefficients, it is possible to see (Fig. 5) that this simple dependence yields the qualitative experimental trend (pink line). However, the definition given in Eq. (4) depends on the average of Li content of the alloy, while MB senses the local environment. We can seek a better agreement if we calculate the local concentration of Li and Si atoms by considering the nearest neighbors of each Si atom for each of the amorphous alloys, as obtained from the averages of the simulations. If we replace into Eq. (5) the C_{Li} and C_{Si} values

obtained from the simulations in this way, we get the cyan dots of Fig. 5, showing an improved agreement with experiment.

IV. CONCLUSIONS

We can summarize the results obtained herein by stating that we have used a recently developed DFTB model to generate the configuration of amorphous Li-Si alloys of different Li contents, covering the usual experimental range. These configurations lead to pair distribution functions that are in excellent agreement with experimental results. When the same configurations are used to predict NMR and Mössbauer spectra at different alloy compositions, also a very good agreement is found with experiment. The present results encourage to use this DFTB method to predict other properties of Li-Si alloys, a promising system in the field of Li-ion battery materials.

ACKNOWLEDGMENTS

This work used computational resources from CCAD-UNC, which is part of SNCAD-MinCyT, Argentina. F.F. acknowledges support from a Ph.D. fellowship from CONICET. We acknowledge financial support from CONICET (28702021010062 3CO, 28702021010119 0CO, 1220200101189CO, PUE/2017), the Agencia Nacional de Promoción Científica y Tecnológica (FONCyT 2020-SERIEA-02139, 2020-SERIEA-03689), and SECyT of the Universidad Nacional de Córdoba.

[1] L. D. Harvey, *Global Warming* (Routledge, New York, 2018).
[2] M. Obrovac and L. Christensen, Structural changes in silicon anodes during lithium insertion/extraction, Electrochem. Solid-State Lett. **7**, A93 (2004).
[3] D. Liu, Z. Shadike, R. Lin, K. Qian, H. Li, K. Li, S. Wang, Q. Yu, M. Liu, S. Ganapathy *et al.*, Review of recent development of *in situ*/operando characterization techniques for lithium battery research, Adv. Mater. **31**, 1806620 (2019).
[4] B. Key, M. Morcrette, J.-M. Tarascon, and C. P. Grey, Pair distribution function analysis and solid state NMR studies of silicon electrodes for lithium ion batteries: Understanding the (de) lithiation mechanisms, J. Am. Chem. Soc. **133**, 503 (2011).
[5] K. Pan, F. Zou, M. Canova, Y. Zhu, and J.-H. Kim, Systematic electrochemical characterizations of Si and SiO anodes for high-capacity Li-ion batteries, J. Power Sources **413**, 20 (2019).
[6] N. Ding, J. Xu, Y. Yao, G. Wegner, X. Fang, C. Chen, and I. Lieberwirth, Determination of the diffusion coefficient of lithium ions in nano-Si, Solid State Ionics **180**, 222 (2009).
[7] B. Key, R. Bhattacharyya, M. Morcrette, V. Seznec, J.-M. Tarascon, and C. P. Grey, Real-time NMR investigations of structural changes in silicon electrodes for lithium-ion batteries, J. Am. Chem. Soc. **131**, 9239 (2009).
[8] M. B. Oviedo, F. Fernandez, M. Otero, E. P. Leiva, and S. A. Paz, Density functional tight-binding model for lithium–silicon alloys, J. Phys. Chem. A **127**, 2637 (2023).
[9] K. Laaziri, S. Kycia, S. Roorda, M. Chicoine, J. L. Robertson, J. Wang, and S. C. Moss, High resolution radial distribution function of pure amorphous silicon, Phys. Rev. Lett. **82**, 3460 (1999).
[10] T. K.-J. Köster, E. Salager, A. J. Morris, B. Key, V. Seznec, M. Morcrette, C. J. Pickard, and C. P. Grey, Resolving the different silicon clusters in $Li_{12}Si_7$ by ^{29}Si and $^{6,7}Li$ solid-state NMR spectroscopy, Angew. Chem., Int. Ed. **50**, 12591 (2011).
[11] K. Ogata, E. Salager, C. Kerr, A. Fraser, C. Ducati, A. J. Morris, S. Hofmann, and C. P. Grey, Revealing lithium–silicide phase transformations in nano-structured silicon-based lithium ion batteries via *in situ* NMR spectroscopy, Nat. Commun. **5**, 3217 (2014).
[12] J. Li, A. Smith, R. Sanderson, T. Hatchard, R. Dunlap, and J. Dahn, *In situ* ^{119}Sn Mössbauer effect study of the reaction of lithium with Si using a Sn probe, J. Electrochem. Soc. **156**, A283 (2009).
[13] X. Wang, S. Tan, X.-Q. Yang, and E. Hu, Pair distribution function analysis: Fundamentals and application to battery materials, Chin. Phys. B **29**, 028802 (2020).
[14] V. Chevrier and J. R. Dahn, First principles model of amorphous silicon lithiation, J. Electrochem. Soc. **156**, A454 (2009).
[15] H. J. Berendsen, J. Postma, W. F. van Gunsteren, A. DiNola, and J. R. Haak, Molecular dynamics with coupling to an external bath, J. Chem. Phys. **81**, 3684 (1984).
[16] B. Hourahine, B. Aradi, V. Blum, F. Bonafé, A. Buccheri, C. Camacho, C. Cevallos, M. Deshaye, T. Dumitrică, A. Dominguez *et al.*, DFTB+, a software package for efficient approximate density functional theory based atomistic simulations, J. Chem. Phys. **152**, 124101 (2020).
[17] See Supplemental Material at http://link.aps.org/supplemental/10.1103/PhysRevB.108.144201 for details of the DFTB method, the calculations to obtain $G(r)$, and a visual explanation of the nearest-neighbor model for predicting NMR spectra.
[18] F. Fernandez, S. A. Paz, M. Otero, D. Barraco, and E. P. Leiva, Characterization of amorphous Li_xSi structures from ReaxFF via accelerated exploration of local minima, Phys. Chem. Chem. Phys. **23**, 16776 (2021).
[19] F. Fernandez, M. Otero, M. B. Oviedo, D. E. Barraco, S. A. Paz, and E. P. Leiva, Structures of the amorphous LiSi system obtained with DFTB model, https://github.com/fernandezfran/DFTB_LiSi_amorphous/, doi:10.5281/zenodo.8274845 (2023).
[20] C.-P. Chou, Y. Nishimura, C.-C. Fan, G. Mazur, S. Irle, and H. A. Witek, Automatized parameterization of DFTB using particle swarm optimization, J. Chem. Theory Comput. **12**, 53 (2016).
[21] M. Wahiduzzaman, A. F. Oliveira, P. Philipsen, L. Zhechkov, E. van Lenthe, H. A. Witek, and T. Heine, DFTB parameters for the periodic table: Part 1, electronic structure, J. Chem. Theory Comput. **9**, 4006 (2013).
[22] G. Seifert, Tight-binding density functional theory: An approximate Kohn-Sham DFT scheme, J. Phys. Chem. A **111**, 5609 (2007).
[23] T. Frauenheim, G. Seifert, M. Elsterner, Z. Hajnal, G. Jungnickel, D. Porezag, S. Suhai, and R. Scholz, A self-consistent charge density-functional based tight-binding method for predictive materials simulations in physics, chemistry and biology, Phys. Status Solidi B **217**, 41 (2000).

[24] M. Elstner, D. Porezag, G. Jungnickel, J. Elsner, M. Haugk, T. Frauenheim, S. Suhai, and G. Seifert, Self-consistent-charge density-functional tight-binding method for simulations of complex materials properties, Phys. Rev. B **58**, 7260 (1998).

[25] R. D. Woods and D. S. Saxon, Diffuse surface optical model for nucleon-nuclei scattering, Phys. Rev. **95**, 577 (1954).

[26] S. J. Billinge, The rise of the x-ray atomic pair distribution function method: a series of fortunate events, Philos. Trans. R. Soc. A **377**, 20180413 (2019).

[27] A. Jain, S. P. Ong, G. Hautier, W. Chen, W. D. Richards, S. Dacek, S. Cholia, D. Gunter, D. Skinner, G. Ceder *et al.*, Commentary: The Materials Project: A materials genome approach to accelerating materials innovation, APL Mater. **1**, 011002 (2013).

[28] T. D. Hatchard, M. N. Obrovac, and J. R. Dahn, A comparison of the reactions of the SiSn, SiAg, and SiZn binary systems with L3i, J. Electrochem. Soc. **153**, A282 (2006).